



NIH PUBLIC ACCESS

Author Manuscript

Med Image Comput Assist Interv. Author manuscript; available in PMC 2015 January 01.

Published in final edited form as:

Med Image Comput Assist Interv. 2014 ; 17(0 3): 313–320.

Human Connectome Module Pattern Detection Using A New Multi-Graph MinMax Cut Model

De Wang¹, Yang Wang², Feiping Nie¹, Jingwen Yan², Weidong Cai³, Andrew J. Saykin², Li Shen², and Heng Huang^{1,*}

¹Computer Science and Engineering, University of Texas at Arlington, TX, USA

²Radiology and Imaging Sciences, Indiana University School of Medicine, IN, USA

³BMIT Research Group, School of IT, University of Sydney, Australia

Abstract

Many recent scientific efforts have been devoted to constructing the human connectome using Diffusion Tensor Imaging (DTI) data for understanding the large-scale brain networks that underlie higher-level cognition in human. However, suitable computational network analysis tools are still lacking in human connectome research. To address this problem, we propose a novel multi-graph min-max cut model to detect the consistent network modules from the brain connectivity networks of all studied subjects. A new multi-graph MinMax cut model is introduced to solve this challenging computational neuroscience problem and the efficient optimization algorithm is derived. In the identified connectome module patterns, each network module shows similar connectivity patterns in all subjects, which potentially associate to specific brain functions shared by all subjects. We validate our method by analyzing the weighted fiber connectivity networks. The promising empirical results demonstrate the effectiveness of our method.

1 Introduction

Advent of diffusion MRI technology has made tremendous progress over the last decade [2] and enables us to use Diffusion Tensor Imaging (DTI) for non-invasive in vivo white matter mapping of the human brain by the inference of axonal fiber pathways from local water diffusion [4]. DTI combined with tractography allows the reconstruction of the major fiber bundles in the brain and also permits the mapping of white matter cortico-cortical and cortico-subcortical projections at high spatial resolution. These studies enable the analysis of the human connectome as organizational principle of the central nervous system.

Understanding the structural basis of functional connectivity patterns requires a comprehensive map of structural connection of the human brain, which has been conceptualized as the human connectome [10]. A connectome is a comprehensive description of the network elements and connections that form the brain. Such clear and comprehensive knowledge of anatomical connections lies at the basis of understanding

*DW, FN, and HH were supported by IIS-1117965, IIS-1302675, IIS-1344152, DBI-1356628. JY, AS, and LS were supported in part by NSF IIS-1117335, NIH UL1 RR025761, U01 AG024904, NIA RC2 AG036535, NIA R01 AG19771, NIH R01 LM011360, and NIA P30 AG1013318S1.

network functions. The connectome can be represented as a large interconnected graph, in which nodes are neuroanatomical regions and synapses are bundles of white matter tracts. The resultant networks exhibit important topological properties such as small-worldness and highly connected hub regions in the posterior medial cortical regions. These studies have accelerated our understandings of human connectome.

Although many network and graph analysis tools have been applied to human connectome studies, most of them focus on analyzing the connectome of each subject individually. How to find the consistent network module patterns (connectome modules) from a group of subjects (*i.e.* a set of regions are connected by similar density of nerve fibers in all subjects) under the same condition (*e.g.* normal or Alzheimer) is important to understand the underlying brain structural and functional mechanisms. The existing research work mainly used the average connectivity networks of all subjects to seek the consistent network modules, however, this straightforward method can easily fail to many conditions. For example, one or two subjects have very strong signals connecting two brain regions, but the rest of subjects have small values on this connectivity. The average connectivity value of all subjects between these two regions can still be large, which indicates a wrong connectivity pattern.

To solve this challenging problem, we propose a novel multi-graph MinMax cut model to identify the consistent network patterns from brain connectivity networks of a group of subjects. Our new approach does the min-max cut on each connectivity network simultaneously. The common connectome patterns are then detected from the dense connected modules. We introduce a new projected gradient optimization algorithm to solve the proposed multi-graph MinMax cut objective. By analyzing the weighted fiber connectivity network from 50 young male adults, we identify six consistent network modules which consistently carry high connectivity among all the subjects. These connectome module patterns potentially associate to the common brain functions shared by all subjects.

2 Methodology

2.1 Consistent Connectivity Patterns

The brain connectome of each subject can be represented as a graph A , in which each node is an ROI (region of interest) in human brain and the weight of each edge is the density of the nerve fibers connecting a pair of nodes. In next section, we will describe the details of brain network construction. Given a group of m subjects under the same condition with n ROIs, we can denote their connectivity networks as A^1, A^2, \dots, A^m , where $A^k \in \mathbb{R}^{n \times n}$ and A_{ij}^k denotes the connectivity of the i -th ROI and the j -th ROI in the k -th subject, $k = 1, \dots, m$, $1 \leq i, j \leq n$.

It is important to discover the common consistent connectivity patterns, *i.e.* a set of ROIs connected by similar density of nerve fibers in all subjects, which are potentially associated to the underlying brain structural and functional mechanisms shared by the subjects. Thus, our goal is to detect the sub-networks which have similar connectivity structures in all or most A^1, A^2, \dots, A^m .

Although there are many graph cut methods to group nodes in the graph, these approaches only work for single graph and cannot find the common connectome patterns. Thus, we propose a novel multi-graph MinMax cut model to group nodes based on their structures in all connectivity networks.

2.2 Multi-Graph MinMax Cut

Given a graph with weight matrix $A \in \mathfrak{R}^{n \times n}$, there are many graph cut methods to group nodes, such as Min Cut, Ratio Cut, Normalized Cut, and MinMax Cut. The MinMax cut can provide the balanced group results to avoid grouping the outlier data together. Thus, MinMax cut is preferred to group nodes in connectome data analysis. However, the traditional MinMax cut only works for single graph. To solve the multiple networks problem, we propose a novel multi-graph MinMax cut model for grouping nodes on multiple graphs simultaneously.

Let $A^v \in \mathfrak{R}^{n \times n}$ denote the v -th network, and D^v are diagonal matrices whose diagonal

elements are $\sum_j a_{ij}^v$. When we perform MinMax cut on the v -th network, we can minimize the following spectral relaxed objective [9]:

$$\min_{(Q^v)^T Q^v = I} \sum_{k=1}^K \frac{(q_k^v)^T D^v q_k^v}{(q_k^v)^T A^v q_k^v}, \quad (1)$$

where $Q^v = [q_1^v, \dots, q_K^v] \in \mathfrak{R}^{n \times K}$ is the group indicator matrix for the v -th network and K is the number of groups.

The straightforward way to group ROIs on all networks is to average the corresponding edge weights to build a new “ensemble” network, and perform the MinMax cut on the new network. However, in such method, some networks have very strong signals in local ROIs will dominate the average network and lead to the wrong connectivity patterns. It is ideal to simultaneously perform the MinMax cut on each network and unify their consistent results.

When the multi-graph MinMax algorithm is performed on all networks, the grouping results in different networks should be unique, *i.e.* the group indicator matrices $Q^{(v)}$ of different networks should share the same one. Therefore, in multi-graph MinMax, we force the group assignment matrices to be the same across different networks, that is, the consensus common group indicator matrix $Q \in \mathfrak{R}^{n \times K}$. Our new Multi-Graph MinMax Cut model (MGMMC) is to solve the following objective:

$$\min_{Q^T Q = I} J(Q) = \sum_{v=1}^m \sum_{k=1}^K \frac{q_k^T D^v q_k}{q_k^T A^v q_k} \quad (2)$$

where m is number of connectivity networks, K is number of clusters. The proposed model is capable of capturing the connectome structures from different networks, and thus expected to get consistent connectivity patterns. It is difficult to solve the objective in Eq. (2) because of the orthonormality constraints. We will derive our optimization algorithm using the projected gradient descent method.

Taking derivative on $J(Q)$ w.r.t. q_k , we get:

$$\frac{\partial J}{\partial q_k} = \sum_{v=1}^m \frac{(q_k^T A^v q_k) D^v q_k - (q_k^T D^v q_k) A^v q_k}{(q_k^T A^v q_k)^2} = \sum_{v=1}^m \frac{1}{q_k^T A^v q_k} D^v q_k - \frac{q_k^T D^v q_k}{(q_k^T A^v q_k)^2} A^v q_k$$

We denote:

$$\alpha^v = \text{diag}\left(\frac{1}{q_1^T A^v q_1}, \dots, \frac{1}{q_K^T A^v q_K}\right), \beta^v = \text{diag}\left(\frac{q_1^T D^v q_1}{(q_1^T A^v q_1)^2}, \dots, \frac{q_K^T D^v q_K}{(q_K^T A^v q_K)^2}\right),$$

where $\text{diag}(x)$ represents a diagonal matrix whose diagonal elements are the elements in vector x .

So Eq. (3) can be rewritten as:

$$\frac{\partial J}{\partial Q} = \sum_{v=1}^m D^v Q \alpha^v - A^v Q \beta^v. \quad (3)$$

Because we have the orthonormal constraint $Q^T Q = I$ in objective, we can use the projected gradient descent method to solve this problem. Given Q , we calculate a new variable H by:

$$H = Q - \tau \left(\sum_{v=1}^m D^v Q \alpha^v - A^v Q \beta^v \right). \quad (4)$$

When H is fixed, we need to solve the following constrained optimization problem:

$$\min_{Q^T Q = I} \|Q - H\|_F^2 \quad (5)$$

Because

$$\|Q - H\|_F^2 = \text{Tr}((Q - H)^T (Q - H)) = \text{Tr}(Q^T Q - 2Q^T H + H^T H), \quad (6)$$

and $Q^T Q = I$, and H is fixed, problem (5) is equivalent to solve the following problem:

$$\max_{Q^T Q = I} \text{Tr}(Q^T H). \quad (7)$$

If the SVD result of H is : $H = U \Sigma V^T$, then the optimal solution of problem (7) can be obtained by:

$$Q = U_K V^T, \quad (8)$$

where U_K is composed of the first K columns of U . Thus, we can iteratively solve H using Eq. (4) and update Q by Eq. (8) till convergence.

3 Human Brain Connectivity Network Construction

In our project, participants included 50 healthy young male adults (age: 24.0 ± 3.2) with no history of neurological or psychiatric disorder. The MRI scans were acquired on a Siemens 3T TIM Trio (Erlangen, Germany) using a 12-channel receive only phased array head coil in combination with a body coil for radio frequency transmission. A SE-EPI DTI sequence was applied using parameters: matrix= 128×128 ; FOV= 256×256 mm; TE/TR=77/8300 ms; 68 transversal slices with 2mm thickness; 48 diffusion directions with gradients $b=1000$ s/mm², and 8 samplings at $b=0$. Each session also included a high resolution T1-weighted MP-RAGE imaging as anatomical reference for subsequent parcellation and co-registration.

The DTI data are analyzed in FSL⁴. DTI preprocessing includes correction for motion and eddy current effects in DTI images. The processed DTI images are then output to Diffusion Toolkit (<http://trackvis.org/>) for fiber tracking, using the streamline tractography algorithm called FACT (fiber assignment by continuous tracking). The FACT algorithm initializes tracks from many seed points and propagates these tracks along the vector of the largest principle axis within each voxel until certain termination criteria are met. In our study, stop angle threshold is set to 35 degree, which means if the angle change between two voxels is greater than 35 degree, the tracking process stops. A spline filtering is then applied to smooth the tracks.

Anatomical parcellation is performed using FreeSurfer 5.1⁵ [7, 5, 6] on the high-resolution T1-weighted anatomical MRI scan acquired with MP-RAGE sequence. The parcellation is an automated operation on each subject to obtain 82 gyral-based ROIs, with 41 cortical ROIs in each hemisphere, one in brainstem. The T1-weighted MRI image is registered to the low resolution b0 image of DTI data using the FLIRT toolbox in FSL, and the warping parameters are applied to the ROIs so that a new set of ROIs in the DTI image space are created. These new ROIs are used for constructing the structural network.

The topological representation of a network is a collection of nodes and edges between pairs of nodes. In constructing the weighted, undirected network, the nodes are chosen to be the 83 registered ROIs obtained from FreeSurfer parcellation. Three different schemes [8, 3] are used to define the edge weight as follows: 1) Weighted: The density of the fibers connecting a pair of nodes, which is the number of tracks between two ROIs divided by the mean volume of the two ROIs; 2) Fiber number: the number of tracks between two ROIs; 3) Fiber length: the length of tracks between two ROIs. Figure 1 shows the pipeline for constructing brain connectivity networks in our experiments.

⁴<http://www.fmrib.ox.ac.uk/fsl.html>

⁵<http://surfer.nmr.mgh.harvard.edu/>

4 Experiments and Discussions

4.1 Experiment Setup

We apply our MGMMC model on the 50 connectivity networks. The parameter group number K is set as 10, and the stepsize τ is set as 0.001 for all experiments. We use the normalized connectivity measure of connectome modules to evaluate the density of detected modules:

$$B_{tt} = \frac{\sum_{v=1}^m s_{tt}^v}{m \cdot n_t^2}, \quad (9)$$

where B_{tt} represents the normalized connectivity of the t -th connectome module, m is the total number of networks used in experiments, n_t is the cardinality of the t -th module C_t (C_t is the set of ROIs contained in the t -th cluster), *i.e.* the number of ROIs in t -th module C_t .

$s_{tt}^v = \sum_{i \in C_t, j \in C_t} A_{ij}^v$ is the connectivity measure of the t -th module in the v -th network.

4.2 Comparison of Connectivity Measures

To demonstrate the effectiveness of our MGMMC model, we compare MGMMC with two methods:

1. MMC performed on the average network, where $G_{avg} = \frac{\sum_{v=1}^m G^v}{m}$.
2. Multi-Modal Spectral Clustering (MMSC)[1], which integrates data from different modality/view to perform spectral clustering.

The connectivity measure are reported in Table 1 and in Figure 2. We can conclude that: for all three types of graph (W, LL, NF), the average connectivity measurements of top 6 modules detected by our MGMMC model are greater than that of modules detected using the two comparison methods. This justifies the effectiveness and advantage of our MGMMC model, which considers the connectivity structures in different graphs. T-test is performed to evaluate the significance of difference of the module connectivity. The p values of the T-test for the six pair comparisons (W, W_avg), (W, W_mmssc), (LL, LL_avg), (LL, LL_mmssc), (NF, NF_avg), (NF, NF_mmssc) are 0.14, 0.04, 0.04, 0.008, 0.03, 0.03. Five out of the six p values are less than 0.05, which means the difference of most of the six pair comparisons are significant in all cases except one. We can also see from Table 1 that: the average connectivity measures of detected connectome modules by using weighted network is the best among three types of networks, and the fiber length (LL) network gets the worst connectivity measures. This shows that the weighted network is the best connectivity measurement.

4.3 Visualization of Detected Modules

We visualize the top 6 connectome modules using weight network detected by MGMMC model in Figure 4.3. Only the first 24 subjects are shown due to space limitation. ROIs contained in each connectome module are listed on the left-side in Figure 4.3. We can see that three pairs of modules are almost symmetric except for one ROI in each pair: module 1 and module 2, module 3 and module 6, module 4 and module 5. This shows that each

connectome module has its counterpart in the other half brain. In Figure 4, we visualize the location of the top 6 connectome modules in human brain.

5 Conclusion

In this paper, we proposed a novel brain connectivity network analysis method by employing the new multi-graph MinMax cut model to identify the consistent connectivity patterns from multiple subjects. We introduced an efficient algorithm to discover such connectivity patterns that are potentially associated to different brain functions of humans. The clinical DTI data were used to construct the brain connectivity networks to validate our methods. Several important highly connected sub-network modules were detected.

References

1. Cai, X.; Nie, F.; Huang, H.; Kamangar, F. Computer Vision and Pattern Recognition (CVPR), 2011 IEEE Conference on. IEEE; 2011. Heterogeneous image feature integration via multi-modal spectral clustering; p. 1977-1984.
2. Catani M, Howard R, Pajevic S, Jones D. Virtual in vivo interactive dissection of white matter fasciculi in the human brain. *Neuroimage*. 2002; 17(1):77-94. [PubMed: 12482069]
3. Cheng H, et al. Optimization of seed density in dti tractography for structural networks. *J Neurosci Methods*. 2012; 203(1):264-72. [PubMed: 21978486]
4. Ciccarelli O, Toosy A, Parker G, Wheeler-Kingshott C, Barker G, Miller D, Thompson A. Diffusion tractography based group mapping of major white-matter pathways in the human brain. *Neuroimage*. 2003; 19(4):1545-1555. [PubMed: 12948710]
5. Dale A, Fischl B, Sereno M. Cortical surface-based analysis. i. segmentation and surface reconstruction. *Neuroimage*. 1999; 9(2):179-94. [PubMed: 9931268]
6. Fischl B, et al. Whole brain segmentation: automated labeling of neuroanatomical structures in the human brain. *Neuron*. 2002; 33(3):341-55. [PubMed: 11832223]
7. Fischl B, Sereno M, Dale A. Cortical surface-based analysis. ii: Inflation, flattening, and a surface-based coordinate system. *Neuroimage*. 1999; 9(2):195-207. [PubMed: 9931269]
8. Hagmann P, Kurant M, Gigandet X, Thiran P, Wedeen VJ, Meuli R, Thiran JP. Mapping human whole-brain structural networks with diffusion MRI. *PLoS One*. 2007; 2(7):e597. [PubMed: 17611629]
9. Nie F, Ding C, Luo D, Huang H. Improved minmax cut graph clustering with nonnegative relaxation. *ECML/PKDD*. 2010:451-466.
10. Sporns O, Tononi G, Kotter R. The human connectome: a structural description of the human brain. *PLoS Comput Biol*. 2005; 1(4):e42. [PubMed: 16201007]

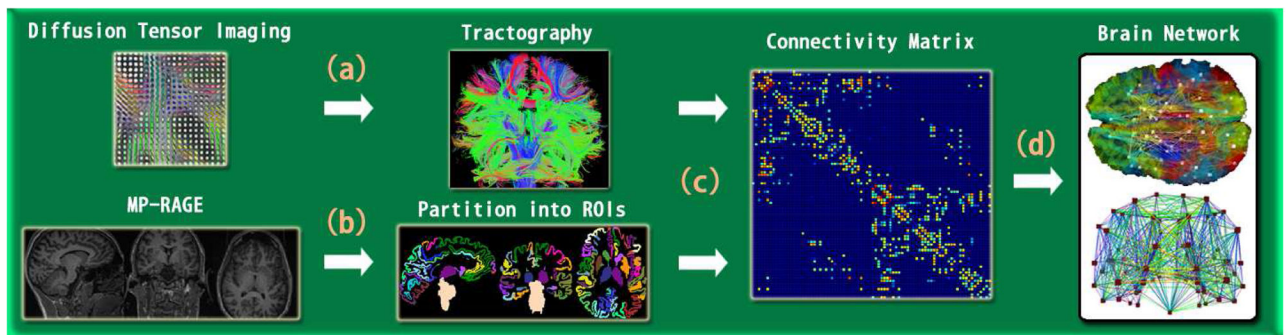
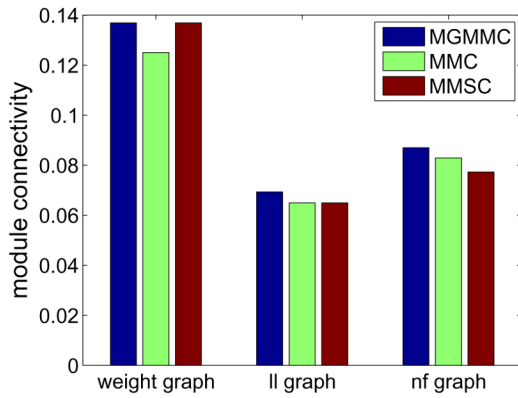
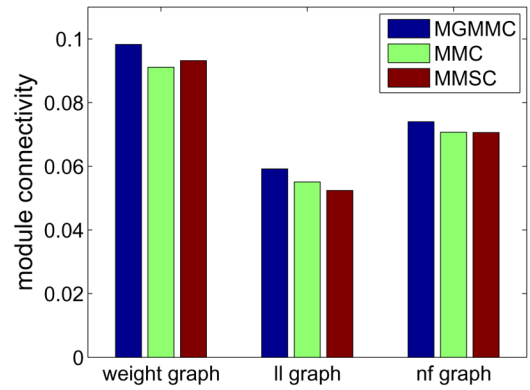


Fig. 1.

Construction of structural connectivity network: (a) Fiber extraction via DTI tractography. (b) ROI definition via brain segmentation and cortical parcellation on MP-RAGE scan. (c) Creation of connectivity matrix A , where $A(i, j)$ stores the connectivity measure between ROI i and ROI j . (d) Visualization of connectivity matrix as a brain network.



(a) Connectivity of the first module



(b) Average connectivity of the top 6 modules

Fig. 2.

The connectivity measure comparisons for three methods.



Fig. 3. The top 6 connectome modules discovered by our MGMMC model. ROIs contained in each connectome module are listed on the left-side. The edge between two nodes denotes there is connection between these two ROIs. Zoom in for clear view.

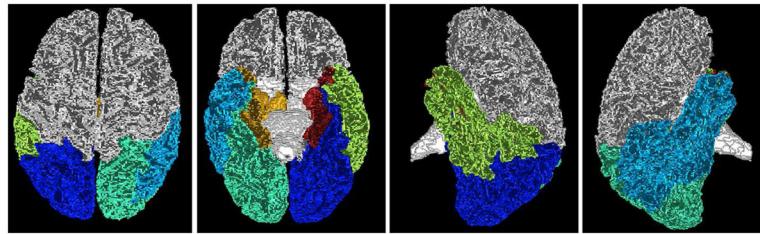


Fig. 4. Location visualization of top 6 connectome modules discovered by MGMMC model from top, bottom, right, left views.

Table 1

B_H for top 6 modules with largest connectivity. W, LL and NF denote the results of using our MGMMC model on the graphs of weighted, fiber length, and fiber number, respectively; W_mmc, LL_mmc, and FN_mmc denote the results of MMC using the average graph; W_mmhc, LL_mmhc, and FN_mmhc denote the results using mmhc method.

Module	W	W_mmc	W_mmhc	LL	LL_mmc	LL_mmhc	NF	NF_mmc	NF_mmhc
1	0.1369	0.1250	0.1369	0.0693	0.0649	0.0649	0.0870	0.0829	0.0773
2	0.1003	0.1136	0.0884	0.0649	0.0636	0.0636	0.0818	0.0765	0.0741
3	0.0971	0.0812	0.0867	0.0607	0.0607	0.0545	0.0765	0.0726	0.0735
4	0.0884	0.0780	0.0865	0.0582	0.0522	0.0522	0.0726	0.0658	0.0709
5	0.0867	0.0780	0.0839	0.0522	0.0495	0.0403	0.0640	0.0638	0.0702
6	0.0805	0.0709	0.0768	0.0495	0.0393	0.0386	0.0624	0.0624	0.0574
Average	0.0983	0.0911	0.0932	0.0592	0.0551	0.0524	0.0740	0.0707	0.0706